13th International Symposium on Turbulence and Shear Flow Phenomena (TSFP13)
Montreal, Canada, June 25-28, 2024

WALL-NORMAL-MICROJET-BASED DRAG REDUCTION OF HIGH REYNOLDS NUMBER TURBULENT BOUNDARY LAYERS

X. Zhang
Center for Turbulence Control
Harbin Institute of Technology (Shenzhen)
Shenzhen 518055, China
zhangxin_fluid@qq.com

X. H. Wei
Center for Turbulence Control
Harbin Institute of Technology (Shenzhen)
Shenzhen 518055, China
weixiaohui17@mails.ucas.edu.cn

E. D. Zhang
Center for Turbulence Control
Harbin Institute of Technology (Shenzhen)
Shenzhen 518055, China
eneast.zhang@connect.polyu.hk

H. F. Wang
School of Civil Engineering
Central South University
Changsha 410075, China
wanghf@csu.edu.cn

Y. Zhou
Center for Turbulence Control
Harbin Institute of Technology (Shenzhen)
Shenzhen 518055, China
yuzhou@hit.edu.cn

ABSTRACT

This work aims to develop a technology to reduce skin friction in the turbulent boundary layer of a high-speed train, which is both effective and efficient even at high friction Reynolds numbers (Re_τ). To this end, a high-resolution force balance has been innovatively developed to measure accurately the drag reduction (DR) over the control area. The arrays of wall-normal microjets through spanwise slits are deployed, which have been demonstrated to be able to yield a significant DR in spite of additional drag due to slit-associated surface roughness. Experiments were carried out with a Re_τ range from 1000 to 18,000. Results obtained indicate that the maximum spatially-averaged DR over the control area may shoot beyond 70%, though the maximum net energy saving occurs when the DR is only 30-40%. This net energy saving grows with increasing free-stream velocity; its maximum may currently reach 25% at 40 m/s. Hotwire and flow visualization data analyses indicate that the microjet blowing lifts up the streamwise vortices in the TBL. Furthermore, the microjets are of zero streamwise momentum, acting to decrease the near-wall streamwise velocity gradient. Both contribute to the appearance of local flow relaminarization and the significant DR.

INTRODUCTION

China Railway is developing a 600 km/h super high-speed maglev train where the rapid rise in drag, predominantly due to skin friction, as the train speed increases is one of the biggest obstacles. Successful development of techniques to reduce skin friction in turbulent boundary layers (TBLs), which are effective and efficient even at very high Reynolds numbers (*Re*), is crucially important for this development.

In the past several decades, a wide variety of drag reduction (DR) methods have been put forward. Passive methods need no external energy input, including riblets, compliant coatings, and superhydrophobic surfaces, etc. The maximum DR of riblets or compliant coatings is rather limited, in general no more than 8% (e.g. Walsh, 1983; Choi et al., 1997). Nature-inspired superhydrophobic surfaces may lead to a DR of up to 80% (e.g. Daniello et al., 2009; Rastegari and Akhavan, 2015). In aviation or shipping industry, even 1% DR brings significant economic benefits. However, the relatively small DR of riblets cannot offset the cost on the initial installation by the manufacturer, the maintenance and cleaning, and the reinstalling of the riblets (Lynch and Klinge, 1991); compliant and superhydrophobic surfaces are not mature enough for the practical applications.

Although limited to low *Re* conditions, active methods have been widely investigated because of their effectiveness in manipulating TBLs and achieving appreciable DR, including spanwise wall oscillation, body force, flexible wall, and streamwise travelling waves, etc. Spanwise wall oscillation, as one of the most promising control schemes for DR, has been comprehensively studied. The spanwise motion tends to disrupt the spatial coherence between near-wall quasi-streamwise vortices (QSVs) and low speed streaks (Baron and Quadrio, 1995), and hence may lead to an over 40% DR and a 19% maximum net energy saving rate *S* at friction Reynolds number $Re_\tau = 1000$ (e.g. Karniadakis and Choi, 2003; Gatti and Quadrio, 2016). The method based on body force recently received a great deal of attention, and is actively studied both numerically and experimentally (e.g. Yao et al., 2018; Cheng et al., 2021a; Duong et al., 2021). The force is utilized to produce either artificial large-scale streamwise vortices or spanwise wall jets, which acts to suppress the transient growth of streak perturbations and then the near-wall turbulence production. The skin-friction drag can be reduced as large as 30% and the maximum *S* is about 17% at $Re_\tau = 3300$. The flexible surfaces of spanwise transversal traveling waves generate a secondary wall-normal velocity field that interacts with QSVs, and as such the turbulence regeneration cycle is intervened, leading to a DR of 50% at Re_τ=440 and 26%

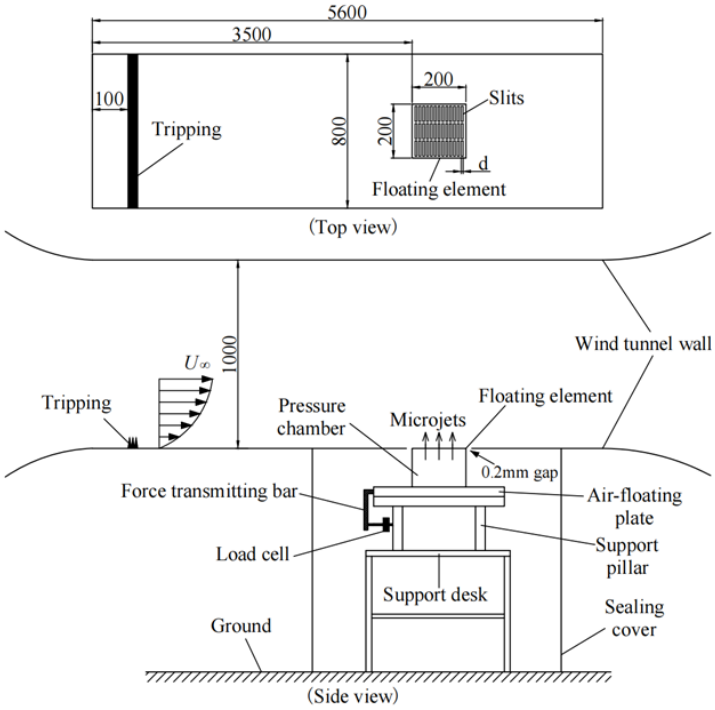

Figure 1. Schematic of the experimental set-up at HIT(SZ) for TBL generation, blowing actuation, and the measurement of skin-friction drag (not to scale; units in mm).

at Re_τ = 1500 (Bai et al., 2014; Li et al., 2018; Mateling et al., 2023). For the streamwise traveling waves of wall-normal blowing/suction and wall deformation, outstanding DR capabilities have been confirmed (Fukagata et al., 2023). The flow could be relaminarized at the optimal parameters in a turbulent channel flow of Re_τ = 180, which resembles the control effect by the means of velocity distortion (Kuhnen et al., 2018), and yields a maximum S of 65% at DR = 69% (Nakanishi et al., 2012). Yet the drag reduction effect for external flows needs further investigations.

Recent advances in the research of wall-bounded turbulent flows at high Re show that large-scale turbulent structures in the outer layer of TBLs become increasingly important with increasing Re in terms of their energy content and their interactions with the smaller scales near the wall. Accordingly, several methods have been developed such that the large-scale structures in the logarithmic region at high Re, instead of the near-wall small-scale structures, are directly controlled. For example, Marusic et al. (2021) used spanwise surface oscillations to reduce drag via a new pathway that involves actuation at frequencies comparable to those of the large-scale eddies farther from the surface. Compared with the previously reported small-scale-based pathway, the new one required significantly less power and the DR grows with Re. On the other hand, caution should be taken to the direct controlling of these outer structures, since the current results show that the suppression of them may not yield an optimistic DR as expected, which is suggested by Yao et al. (2018) that the small scales may also be concomitantly altered by the nonlinear scale interaction.

Wall-normal blowing control, which was first considered for the cooling of surfaces exposed to high-temperature flows, has been extensively reported to be able to reduce skin-friction drag with relatively small blowing intensities. This control strategy essentially does not have to counteract or couple with the near-wall or outer-layer turbulent structures, which is perhaps more applicable than the above reviewed actuations that need complicated microelectromechanical systems. A significant advancement in this field was the micro-blowing technique developed by Hwang (1997), who created relatively smooth perforated surfaces that had low unblown skin friction. Since then, experimental and numerical campaigns have been undertaken to study the blowing control from different aspects, and a number of valuable and insightful results have been reported. Kametani and Fukagata (2011) concluded that uniform blowing reduces friction drag while enhances turbulence by the means of direct numerical simulation. Kornilov (2015) emphasized that a surface consisting of blowing and non-blowing regions interlaced in the streamwise direction could further reduce friction drag. Cheng et al. (2021b) experimentally investigated the control performance of wall-normal blowing through one array of streamwise slits in a TBL of Re_τ = 570. They observed a local DR over 70% and the DR persisted up to 500 wall units downstream of the slits.

In spite of the previous numerous efforts devoted to DR using blowing, a number of issues have yet to be resolved. Firstly, how does the Reynolds number, especially when Re is high, influence the control performance, not only DR but also the control efficiency, when a blowing technique is deployed. This issue has to be addressed before a developed technique could be applied in practical engineering. Secondly, Cheng et al. (2021b) managed to measure the local DR downstream of the blowing through a slit array, whereas the DR where the actuation or blowing takes place could not be determined. Then, can a technique be developed to capture the DR of the actuation area? This work aims to address the above issues.

EXPERIMENTAL DETAILS

Experiments are carried out in the closed-circuit wind tunnel at Harbin Institute of Technology (Shenzhen) in China. For higher *Re*, experiments are also conducted in the closed-circuit wind tunnel at Central South University, which is 15 m long and has the maximum free-stream velocity (U_∞) of 94 m/s. The turbulent boundary layer is generated over the bottom wall of wind tunnel, as shown in figure 1. A 35 mm wide stripe of P40 grit sandpaper is used for tripping. The maximum Re_τ of the experiments is 18,000 (U_∞ = 66 m/s); to the authors' best knowledge, this is the highest Re_τ reported in the literature regarding TBL control.

To measure directly the time-averaged skin-friction drag $\bar{F}$ over the blowing control area, where the overbar denotes time averaging, we substantially redesigned our previously developed floating-element force balance via employing air bearings (Cheng et al., 2021a,c; Wei et al., 2024). The friction force over the control area is in the order of $10^{-2\sim3}$ N, and is amplified by up to 10 times by a lever mechanism so that its small variation could be captured by the loadcell that has a maximum rated load of 0.5 N (figure 1). Following Cheng et al. (2021a,c), the balance is calibrated using both Clauser chart method and calibration weights. It is verified that the balance-measured friction coefficient deviates by no more than 2% from the Coles–Fernholz correlation (Nagib et al., 2007). The uncertainty of drag force determined by the standard deviation of seven repeated measurements is estimated to be 2% at Re_τ = 5500. Additionally, the comparison of the measurement resolution of different force balances is well documented (Cheng et al., 2021c). In summary, the present balance is able to capture reliably smaller wall shear stress, in the order of 10^{-4} N, than other balances.

In this study, the arrays of wall-normal microjets through spanwise slits are deployed, which has been proven to be more effective at high *Re* than the previous microjets through streamwise slits whose DR declines with *Re* (Cheng et al., 2021b). The microjet actuator consists of a square plate machined with spanwise slit arrays and a pressure chamber, which is placed on the floating element of force balance with the plate flush with wind tunnel wall, as depicted in figure 1. The slit width and depth are determined to be 0.25 and 2 mm, respectively, which are the optimum geometric parameters; the porosity is 15%, as suggested by Hwang (1997). Steady microjets through the slits are deployed. It is worth pointing out that this investigation is undertaken with a view to developing a DR technology for the 600 km/h super high-speed maglev train. While providing possibly a higher efficiency than steady forcing (Zhang et al., 2022), unsteady forcing may require a quite high actuating frequency given high Reynolds number TBLs on top of more complex engineering structures, which may not be practically feasible.

The velocity signals of TBLs are obtained by hot-wire anemometry (Dantec Streamline Pro) with the diameter of sensing element 2.5 μm. Following Samie et al. (2018), the nondimensional sampling frequency $f_s^+ \approx 1.8$ and the sampling time *T* at each location of a TBL is given in terms of boundary layer turnovers TU_∞/δ = 6000-8000. The superscript '+' in this study denotes the normalization by the inner scales in the absence of control. The measurement position is at the midspan and 130 wall units downstream of the trailing edge of microjet arrays. This hot-wire probe is mounted on a computer-controlled three-dimensional traversing mechanism, whose spatial resolution is 3.125 μm along each spatial direction.

RESULTS AND DISCUSSION

Figure 2 depicts the dependence of drag change δ_F over the control area on microjet intensity C_b. The δ_F is defined as $(\bar{F}_{on} - \bar{F}_{off}) / \bar{F}_{off}$ and C_b is v_b/U_∞, where the subscripts 'on' and 'off' denote the values with and without control, respectively, and v_b is the average blowing speed over the control area. Drag reduction corresponds to the negative values of δ_F and drag increase to the positive. It is shown that all the DR data of Re_τ ranging from 1000 to 18,000 collapse reasonably well as the abscissa is outer-scale normalized, which implies that the method of microjet arrays can be *Re* independent, i.e., the DR keeps nearly constant at a given C_b in spite of different *Re*. Moreover, the DR rises monotonously with C_b, and a spatially-averaged DR beyond 70% may be achieved once C_b exceeds 0.007, even at an application-level Re_τ = 18,000. The DR approaches 100% given C_b > 0.01, which is the case when the fluid of the microjets totally covers the surface of the control area and the surface is thus isolated from the TBL. Besides, the values of δ_F at C_b = 0 are larger than zero, around 10%, which indicates the additional drag rising from the spanwise slits is relatively small compared to the noticeable DR.

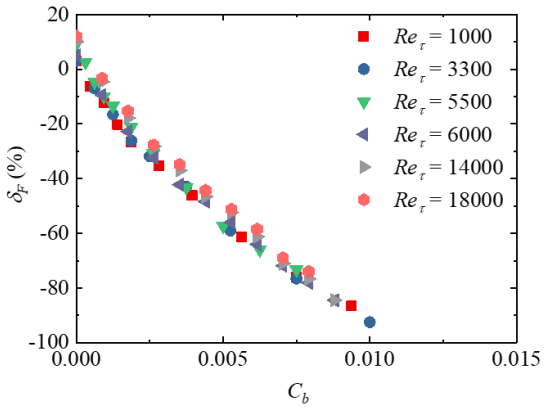

Figure 2. Dependence of drag change δ_F on microjet intensity C_b, where $C_b = v_b / U_\infty$ and v_b is the average blowing speed over the control area.

Figure 3 shows the comparisons of inner-normalized mean velocity $\overline{U^+}$ and turbulence intensity u^+_{rms} profiles between three cases, i.e., the smooth surface, uncontrolled (with slits), and controlled (70% DR), at two Re_τ = 580 and 4700. The left panels in figure 3 are for low *Re*; as such, the hot-wire can capture the signals as close as the wall-normal position of $y^+ = 2$, where the wall effect is tolerable. It is worth noting that the necessity of the measurements in viscous sublayer allows for the fact that the control of microjets takes place at the wall, which indicates the information in the near-wall region will be helpful to study its control mechanism. The data of low *Re* is first discussed. On smooth surface, the mean velocity profile follows the law of the wall for a fully developed TBL, showing a linear near-wall region for $y^+ < 5$ and a logarithmic region for $30 < y^+ < 170$. In the presence of slits, the TBL is hardly impacted, implying possibly that the TBL perceives the slits (width < 2 wall units) as nearly smooth. Once control is activated, the mean velocity of $y^+ < 180$ and turbulence intensity of $y^+ < 10$ are both dramatically reduced, which is beneficial to the significant DR.

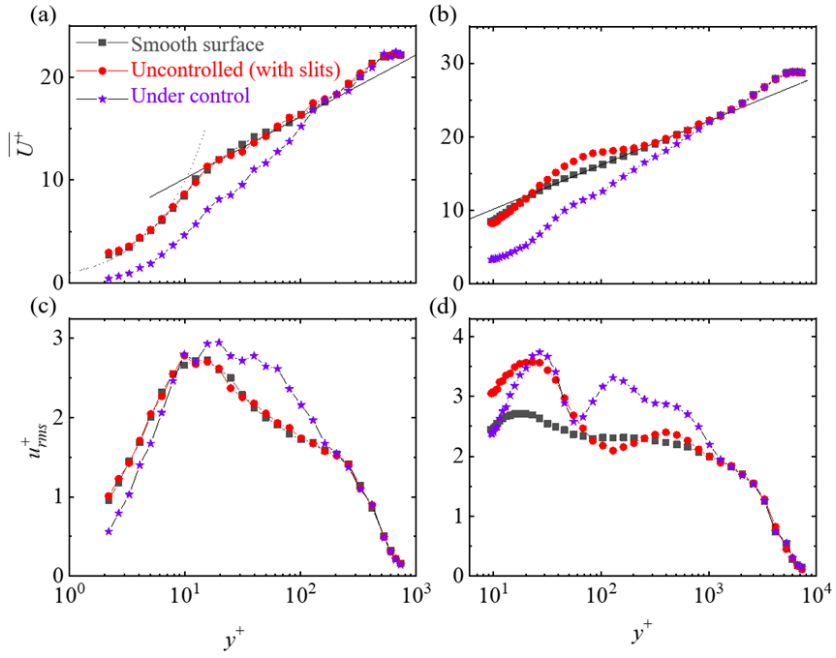

Figure 3. Variations in inner-normalized mean velocity $\overline{U^+}$ (a, b) and turbulence intensity u^+_{rms} (c, d) profiles under control; panels (a, c) for Re_τ = 570 and panels (b, d) for Re_τ = 4 800. Measured at the midspan and 130 wall units downstream of the trailing edge of microjet arrays. Scaled with canonical u_τ. The dotted and straight lines indicate $\overline{U^+} = y^+$ and the log law $\overline{U^+} = 1/0.384\ln(y^+) + 4.17$, respectively. Microjet intensity C_b = 0.007, corresponding to DR ≈ 70%.

These profile changes are essentially attributed to the injected fluid of microjets, whose streamwise momentum is zero and velocity fluctuation is weak. Another observation is that the inner peak in the turbulence intensity profile shifts outwards under control, from y^+ = 14 to 19. It is well known that turbulence intensity is closely associated with QSVs (Wallace, 2016). The shift of the peak therefore implies that the QSVs are lifted up due to the existence of the microjets on the wall. As for the turbulence intensity of $y^+ > 10$, it first surpasses the uncontrolled counterpart and then recovers to the normal state at $y^+ \approx 180$. The strengthened turbulence intensity is a general characteristic in the control using mass injection, which is related to the growing QSVs and will be discussed in the following part of energy spectrum analysis.

Some differences arise as *Re* goes up (figure 3b,d). In contrast to the low *Re*, the slits on surface impose stronger influence on the TBL at high *Re*. With respect to the mean velocity, a bump appears in the log region, centered at $y^+ \approx 120$. The profile of turbulence intensity is also greatly altered: not only the magnitude of the inner peak is much higher, but its location is slightly lifted up and an apparent outer peak at $y^+ \approx$ 400 emerges accompanied with a decline at $y^+ \approx 130$. It is the large nondimensional slit width (> 16 wall units) under high *Re* that gives rise to these changes, which may force the fluid automatically coming in and out through the slits to behave like synthetic jets. The TBL is thus strongly disturbed and more chaotic. Under control, the variations of the profiles are similar to those of the low *Re*, while the influenced range of the TBL is deeper, up to $y^+ \approx 1000$, partly because of their different nondimensional control areas. Besides, the microjets prompt another high-energy outer peak of turbulence intensity appearing at $y^+ \approx 120$, which is merely a little lower than the inner peak. Compared with the low *Re* where the outer peak is not so obvious, the strong outer peak is speculated to result from the interactions between the injected mass and the energetic large-scale structures of high *Re*.

Smoke-wire flow visualizations is conducted at a low Reynolds number Re_τ = 420 in order to gain some insight into the flow physics and DR mechanism behind the observed DR. A smoke-wire, as indicated by a red-colored thick line, is placed at y^+ = 3 and the flow is illuminated in a wall-parallel plane of y^+ = 4. Figure 4 compares the typical images of the instantaneous flow structures captured with and without control. In the absence of control when the wire is placed at the leading edge of the control area (figure 4a), the dark- and white-color or high- and low-speed streaks occur rather randomly, and the average spanwise spacing between low-speed streaks is approximately 100 wall units, as expected. Once control is activated, as shown in figure 4(b), the randomly occurring streaky structures disappear, over a longitudinal extent of about 120 wall units, downstream of the smoke-wire. Instead, we see rather stabilized smoke filaments, an indicator of local relaminarization. It is worth pointing out that the flow relaminarization probably takes place over the entire actuation area. As the smoke wire is moved downstream by 120 wall units (figure 4c), the stabilized filaments occur again downstream. The flow relaminarization is fully consistent with the phenomenon of the lifted QSVs and the substantially reduced friction drag. The observed chaotic flow further downstream may result from the fact that the smoke is gradually lifted up from the wall due to association of a higher temperature and the blowing control effect.

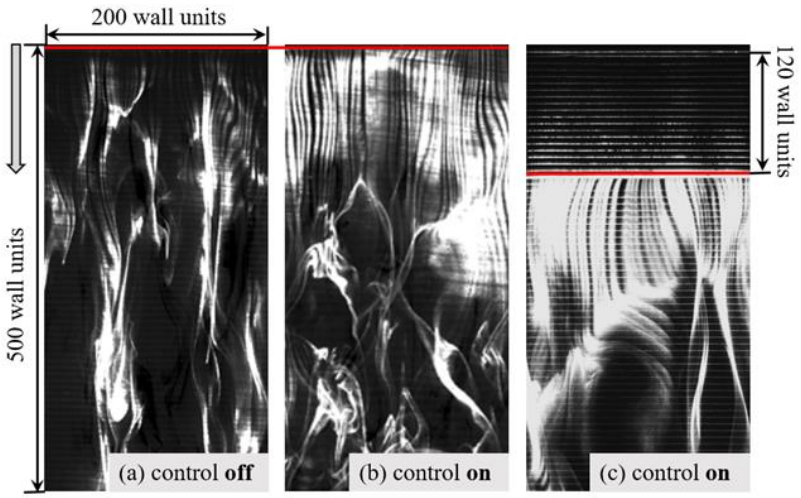

Figure 4. Typical photographs of the instantaneous flow structures captured at Re_τ = 420 (U_∞ = 1.8 m/s) in the wall-parallel plane of y^+ = 4 by smoke-wire visualization: (a) uncontrolled, (b) controlled with smoke wire placed at the leading edge of microjet area, (c) controlled with smoke wire placed at 120 wall units downstream of the leading edge. Control parameters: C_b = 0.007, DR ≈ 70%. Smoke-wire is denoted by red line and the spanwise slits are barely visible in the figures.

Net-energy-saving rate S is an important parameter to be evaluated to determine the efficiency of a DR technique. The S is defined as

$$S = (-C_{f0} \times \delta_F - C_{wb})/\, C_{f0} \qquad (1)$$

where C_{f0} is the spatially-averaged friction coefficient over the control area for uncontrolled flow and $C_{wb} = \Delta C_p \times C_b + C_b^3$ represents the power required to generate blowing jets. The C_{wb} consists of two parts, i.e., the pressure loss due to the pressure difference between pressure chamber and TBL, $\Delta C_p \times C_b$, and the kinetic energy of microjets, C_b^3, where $\Delta C_p = \Delta p/0.5\rho U_\infty^2$ is the pressure coefficient across the perforated plates; Δp is proportional to v_b. It has been found that the latter term is negligibly small, due to weak microjet intensity, compared to the former. The net-energy saving is achieved when $S > 0$, that is, the energy saved is larger than the energy input.

Figure 5 presents the dependence of S on C_b for different U_∞ and Re_τ. Evidently, the maximum S, S_{max}, rises with increasing U_∞; however, S_{max} shows little dependence on Re_τ. Additionally, S_{max} rises with its corresponding C_b and hence DR increasing. S_{max} increases from 5% to 15% when U_∞ ranges from 5 m/s to 66 m/s, at which the DR is 20-30%. The observation is not unexpected. The input control energy $\Delta p \times v_b \propto v_b^2 = C_b^2 \times U_\infty^2$, that is, the input energy is proportional to U_∞^2 for given C_b. On the other hand, it is known that the skin-friction drag is proportional to U_∞^2, and thus the saved energy from DR is proportional to U_∞^3. Naturally, S_{max} rises with increasing U_∞.

In the interest of higher control efficiency, an optimization work on the streamwise spacing between spanwise slits is conducted. Surprisingly, when the spacing is enlarged from 1.7 mm to the optimum value of about 6 mm, corresponding to 500 wall units at the working speed of 40 m/s or Re_t = 5500, both DR and S are profoundly enhanced, i.e., this optimum slit spacing leads to a maximum S of up to 25% when the DR is 37% at C_b = 0.0018, whereas under the same conditions the S and DR are 10% and 18%, respectively, before the optimization. This efficiency enhancement is supposed to benefit from the DR effect that still lasts for a period downstream of each microjet, which is important to be taken into account in terms of the practical usefulness of this kind of control method

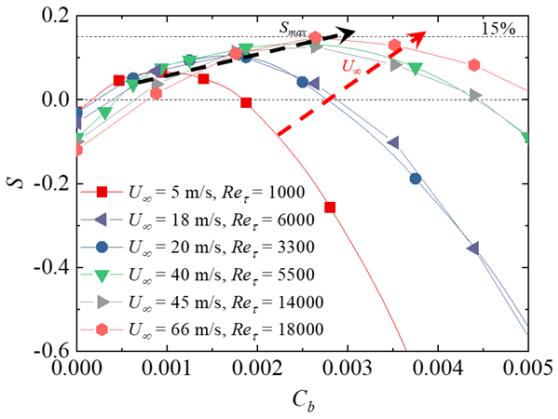

Figure 5. Dependence of net energy saving rate S on C_b.

CONCLUSIONS

1. The arrays of wall-normal microjets through spanwise slits have been deployed to manipulate the TBLs of Re_τ = 1,000-18,000. The drag variation in the control area is captured using our innovative high-resolution force balance. In spite of the additional drag of about 10% from the slits, the spatially-averaged DR over 70%, compared with a smooth surface, is achievable with an average blowing speed of no more than 0.7% of U_∞ for all Re_τ examined.

2. A positive net energy saving rate S is obtained, which shows an appreciable dependence on U_∞. It has been found that the maximum S rises with increasing U_∞, not necessarily with Re_τ. This is because the energy saved from DR and the input

control energy are directly proportional to U_∞^3 and U_∞^2, respectively. A maximum S may reach 15% at 66 m/s and Re_τ = 18,000, while a more encouraging maximum S of 25% is achieved at 40 m/s and Re_τ = 5500 by optimizing the streamwise spacing between spanwise slits, when the DR is 37%.

3. The DR mechanisms are proposed. Hotwire data and flow visualization analyses indicate that the microjet blowing lifts up the streamwise vortices and meanwhile prevents sweeping events from reaching the wall. Furthermore, the microjets are of zero-streamwise-momentum, acting to decrease the near-wall streamwise velocity gradient. The two mechanisms are both responsible for the disappearance of natural streaky structures and the exhibition of local flow relaminarization.

ACKNOWLEDGEMENT

YZ wishes to acknowledge support given to him from CRRC Qingdao Sifang Co. Ltd. through contract SF/GY-梁字-2021-244, NSFC through Grant 91952204 and from the Research Grants Council of Shenzhen Government through grant JCYJ20210324132816040.

REFERENCES

Bai, H. L., Zhou, Y., Zhang, W. G., Xu, S. J., Wang, Y., and Antonia, R. A., 2014, "Active control of a turbulent boundary layer based on local surface perturbation", *Journal of Fluid Mechanics*, Vol. 750, pp. 316-354.

Baron, A., and Quadrio, M., 1995, "Turbulent drag reduction by spanwise wall oscillations", *Applied Scientific Research*, Vol. 55, pp. 311-326.

Cheng, X. Q., Wong, C. W., Hussain, F., Schroeder, W., and Zhou, Y., 2021a, "Flat plate drag reduction using plasma-generated streamwise vortices", *Journal of Fluid Mechanics*, Vol. 918, pp. A24.

Cheng, X. Q., Qiao, Z. X., Zhang, X., Quadrio, M., and Zhou, Y., 2021b, "Skin-friction reduction using periodic blowing through streamwise slits", *Journal of Fluid Mechanics*, Vol. 920, pp. A50.

Cheng, X. Q., Wong, C. W., and Zhou, Y., 2021c, "A high-resolution floating-element force balance for friction drag measurement", *Measurement Science and Technology*, Vol. 32, pp. 035301.

Choi, K. S., Yang, X., Clayton, B. R., Glover, E. J., Atlar, M., Semenov, B. N., and Kulik, V. M., 1997, "Turbulent drag reduction using compliant surfaces", *Proceedings of the Royal Society a-Mathematical Physical and Engineering Sciences*, Vol. 453, pp. 2229-2240.

Daniello, R. J., Waterhouse, N. E., and Rothstein, J. P., 2009, "Drag reduction in turbulent flows over superhydrophobic surfaces", *Physics of Fluids*, Vol. 21, pp. 085103.

Duong, A. H., Corke, T. C., and Thomas, F. O., 2021, "Characteristics of drag-reduced turbulent boundary layers with pulsed-direct-current plasma actuation", *Journal of Fluid Mechanics*, Vol. 915, pp. A113.

Fukagata, K., Iwamoto, K., and Hasegawa, Y., 2023, "Turbulent drag reduction by streamwise traveling waves of wall-normal forcing", *Annual Review of Fluid Mechanics*, Vol. 56, pp. null.

Gatti, D., and Quadrio, M., 2016, "Reynolds-number dependence of turbulent skin-friction drag reduction induced by spanwise forcing", *Journal of Fluid Mechanics*, Vol. 802, pp. 553-582.

Hwang, D. P., 1997, "A proof of concept experiment for reducing skin friction by using a micro-blowing technique", *AIAA Paper*, 97-0546.

Kametani, Y., and Fukagata, K., 2011, "Direct numerical simulation of spatially developing turbulent boundary layers with uniform blowing or suction", *Journal of Fluid Mechanics*, Vol. 681, pp. 154-172.

Karniadakis, G. E., and Choi, K. S., 2003, "Mechanisms on transverse motions in turbulent wall flows", *Annual Review of Fluid Mechanics*, Vol. 35, pp. 45-62.

Kornilov, V. I., 2015, "Current state and prospects of researches on the control of turbulent boundary layer by air blowing", *Progress In Aerospace Sciences*, Vol. 76, pp. 1-23.

Kuhnen, J., Song, B. F., Scarselli, D., Budanur, N. B., Riedl, M., Willis, A. P., Avila, M., and Hof, B., 2018, "Destabilizing turbulence in pipe flow", *Nature Physics*, Vol. 14, pp. 386-390.

Li, W. F., Roggenkamp, D., Hecken, T., Jessen, W., Klaas, M., and Schroder, W., 2018, "Parametric investigation of friction drag reduction in turbulent flow over a flexible wall undergoing spanwise transversal traveling waves", *Experiments In Fluids*, Vol. 59, pp. 105.

Lynch, F. T., and Klinge, M. D., 1991, "Some practical aspects of viscous drag reduction concepts", *SAE Paper*, 912129.

Marusic, I., Chandran, D., Rouhi, A., Fu, M. K., Wine, D., Holloway, B., Chung, D., and Smits, A. J., 2021, "An energy-efficient pathway to turbulent drag reduction", *Nature Communications*, Vol. 12, pp. 5805.

Mateling, E., Albers, M., and Schroder, W., 2023, "How spanwise travelling transversal surface waves change the near-wall flow", *Journal of Fluid Mechanics*, Vol. 957, pp. A30.

Nagib, H. M., Chauhan, K. A., and Monkewitz, P. A., 2007, "Approach to an asymptotic state for zero pressure gradient turbulent boundary layers", *Philosophical Transactions of the Royal Society a-Mathematical Physical and Engineering Sciences*, Vol. 365, pp. 755-770.

Nakanishi, R., Mamori, H., and Fukagata, K., 2012, "Relaminarization of turbulent channel flow using traveling wave-like wall deformation", *International Journal of Heat and Fluid Flow*, Vol. 35, pp. 152-159.

Rastegari, A., and Akhavan, R., 2015, "On the mechanism of turbulent drag reduction with super-hydrophobic surfaces", *Journal of Fluid Mechanics*, Vol. 773, pp. R4.

Samie, M., Marusic, I., Hutchins, N., Fu, M. K., Fan, Y., Hultmark, M., and Smits, A. J., 2018, "Fully resolved measurements of turbulent boundary layer flows up to Re_t=20 000", *Journal of Fluid Mechanics*, Vol. 851, pp. 391-415.

Wallace, J. M., 2016, "Quadrant analysis in turbulence research: history and evolution", *Annual Review of Fluid Mechanics*, Vol. 48, pp. 131-158.

Walsh, M. J., 1983, "Riblets as a viscous drag reduction technique", *AIAA Journal*, Vol. 21, pp. 485-486.

Wei, X., Zhang, X., Chen, J., and Zhou, Y., 2024, "An Air-Bearing Floating-Element Force Balance for Friction Drag Measurement", *Journal of Fluids Engineering*, Vol. 146, pp. 061501.

Yao, J., Chen, X., and Hussain, F., 2018, "Drag control in wall-bounded turbulent flows via spanwise opposed wall-jet forcing", *Journal of Fluid Mechanics*, Vol. 852, pp. 678-709.

Zhang, X., Wong, C. W., Cheng, X. Q., and Zhou, Y., 2022, "Dependence of skin-friction reduction on the geometric parameters of blowing jet array", *Physics of Fluids*, Vol. 34, pp. 105125.